Received 18 July 2019; revised 5 September 2019; accepted 18 September 2019. Date of publication 25 September 2019; date of current version 6 December 2019. The review of this article was arranged by Editor N. Raghavan.

*Digital Object Identifier 10.1109/JEDS.2019.2943609*

# High Hall-Effect Mobility of Large-Area Atomic-Layered Polycrystalline $ZrS_2$ Film Using UHV RF Magnetron Sputtering and Sulfurization

**MASAYA HAMADA, KENTARO MATSUURA, TAKURO SAKAMOTO, IRIYA MUNETA (Member, IEEE), TAKUYA HOSHII (Member, IEEE), KUNIYUKI KAKUSHIMA (Member, IEEE), KAZUO TSUTSUI (Senior Member, IEEE), AND HITOSHI WAKABAYASHI (Member, IEEE)**

Department of Electrical and Electronic Engineering, Tokyo Institute of Technology, Yokohama 226-8503, Japan.

CORRESPONDING AUTHOR: M. HAMADA (e-mail: hamada.m.af@m.titech.ac.jp)

This work was supported in part by the Japan Science and Technology Agency Core Research for Evolutionary Science and Technology (JST CREST) under Grant JPMJCR16F4, and in part by Japan Science and Technology Agency Center of Innovation (JST COI) under Grant JPMJCE1309.

**ABSTRACT** A high Hall-effect mobility of 1,250 $cm^2V^1s^{-1}$ is achieved in $ZrS_2$ film as a two-dimensional semiconductor. A large-area atomic-layered polycrystalline $ZrS_2$ film was obtained by sputtering and sulfurization. It was confirmed that a layered $ZrS_2$ film on a $SiO_2$/Si substrate was successfully achieved by a high-temperature sputtering and sulfur compensation process. We demonstrated that the Hall-effect mobility and the carrier density were greatly improved to 1,250 $cm^2V^{-1}s^{-1}$ and 8.5 x $10^{17}$ $cm^{-3}$, simultaneously. High-mobility two-dimensional $ZrS_2$ film is a strong candidate for advanced MISFETs.

**INDEX TERMS** Transition metal dichalcogenide (TMDC), zirconium disulfide ($ZrS_2$), radio-frequency magnetron sputtering, sulfur vapor annealing.

## I. INTRODUCTION

Transition metal dichalcogenides (TMDCs; general formula $MX_2$, where M = Mo, W, Sn, Hf, Zr, Pt, etc., and X = S, Se, Te, etc.), which are layered materials, have attracted much attention in recent years. They have been reported on high mobility despite atomic-level thickness, a moderate band gap, and unique optical and physical properties [1]–[28]. They are classified into two types of crystal structures, groups VIB and IVB, as shown in Figs. 1 and 2. Among VIB TMDCs, a molybdenum disulfide ($MoS_2$) film has been widely investigated [5]–[30]; however, its mobility is not much higher than that of silicon. On the other hand, the mobilities of group IVB TMDCs are higher than those of the VIB type [1]–[4]. Also, sulfide-based group IVB TMDCs are relatively stable compared to selenium- and tellurium-based TMDC films. Furthermore, for hafnium disulfide film, one preliminary finding is that it is difficult to prevent its oxidation. Therefore, a zirconium disulfide ($ZrS_2$) film seems to be a suitable candidate, having a calculated mobility of 1,200 $cm^2$ $V^{-1}$ $s^{-1}$, a moderate band gap of 1.08 eV, and good optical characteristics [1], [2], [31]–[33]. A previous report speculated that $ZrS_2$-based tunneling field-effect transistors (tFETs) have a high current density of ~ 800 μA/μm, which is ~ $10^2$ times higher than that of $MoS_2$ film [34]. Recently, $ZrS_2$ films formed by chemical vapor deposition (CVD) and exfoliation have been reported. However, their films have low coverage and a mobility of ~ 1.1 $cm^2$ $V^{-1}$ $s^{-1}$ [35]–[38]. Industrial applications of $ZrS_2$ film require a formation with a large area and high quality. Our previous reports confirmed that a layered $MoS_2$ film with a large area was successfully formed on a $SiO_2$ film, and that a sulfurization process enhanced the electrical properties of the $MoS_2$ film [39]–[44].

In this study, $ZrS_2$ film formation is investigated by using a sputtering and sulfurization process for the first time.

## II. EXPERIMENTAL METHODS

$SiO_2$/Si is used as a base substrate and cleaned with a wet process using piranha solution. $ZrS_2$ films were formed by an ultra-high vacuum (UHV) radio frequency (RF) magnetron sputtering tool with a $ZrS_2$ target of 99% purity, as illustrated in Fig. 3(a). The sputtering parameters were

This work is licensed under a Creative Commons Attribution 4.0 License. For more information, see http://creativecommons.org/licenses/by/4.0/

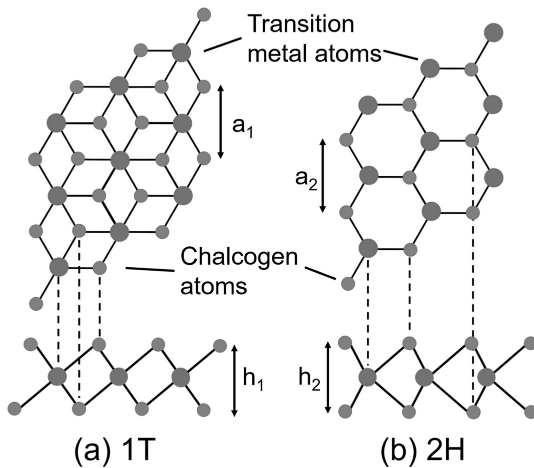


**FIGURE 1.** TMDC layer structure types of (a) 1T and (b) 2H, in which $MX_2$ consists of transition metals (M) of Mo, W, Hf, Zr, etc, and chalcogens (X) of S, Se, Te, etc.

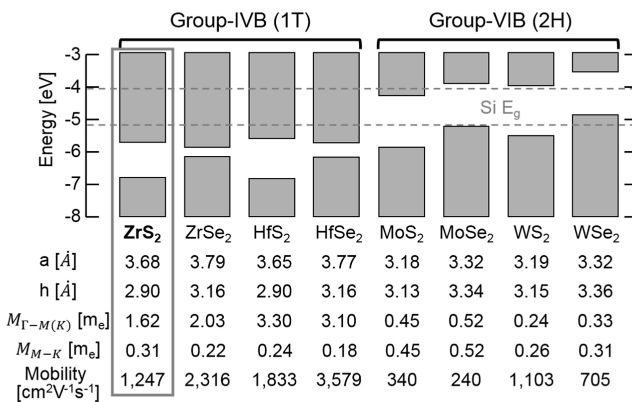


| | ZrS2 | ZrSe2 | HfS2 | HfSe2 | MoS2 | MoSe2 | WS2 | WSe2 |
|---|---|---|---|---|---|---|---|---|
| a [Å] | 3.68 | 3.79 | 3.65 | 3.77 | 3.18 | 3.32 | 3.19 | 3.32 |
| h [Å] | 2.90 | 3.16 | 2.90 | 3.16 | 3.13 | 3.34 | 3.15 | 3.36 |
| $M_{\Gamma-M(K)}$ [$m_e$] | 1.62 | 2.03 | 3.30 | 3.10 | 0.45 | 0.52 | 0.24 | 0.33 |
| $M_{M-K}$ [$m_e$] | 0.31 | 0.22 | 0.24 | 0.18 | 0.45 | 0.52 | 0.26 | 0.31 |
| Mobility [$cm^2V^{-1}s^{-1}$] | 1,247 | 2,316 | 1,833 | 3,579 | 340 | 240 | 1,103 | 705 |

**FIGURE 2.** Band alignment and mobilities of monolayer TMDCs with position of valence band maximum and conduction band minimum. Effective mass values in the Γ-M and Γ-K directions have been reported [1]–[2]. High mobility can be expected among group IVB TMDCs in which $ZrS_2$ film is expected to be relatively stable compared to others in group IVB.

substrate temperatures from 200 to 400°C, argon pressures from 0.35 to 0.75 Pa, sputtering powers from 50 to 90 W, and a distance of 150 mm between the $ZrS_2$ target and Si substrate. Fig. 3 (b) illustrates a sulfur vapor annealing furnace with two zones in argon flow under 100 Pa for sulfur compensation. Sulfur powder was placed in the first heating zone at 250°C for 40 min, and sample wafers were placed in a second heating zone heated from 500 to 700°C for 10-60 min. The Raman spectroscopy with a laser wavelength of 532 nm at 1.5 W and the Hall-effect measurements were performed with 10 times per each samples for whole coupon consisting of 2 cm x 2 cm.

## III. RESULTS AND DISCUSSION

Figure 4 shows the Raman spectra of $ZrS_2$ films with various thicknesses. The $E_{2g}^1$ and $A_{1g}$ peak intensities of $ZrS_2$ film are observed at 248 and 331 $cm^{-1}$ respectively, consistent with previous reports [45], [46]. In the case of $ZrS_2$ film, the $E_{2g}^1$ peak is very small compared to the $A_{1g}$ peak

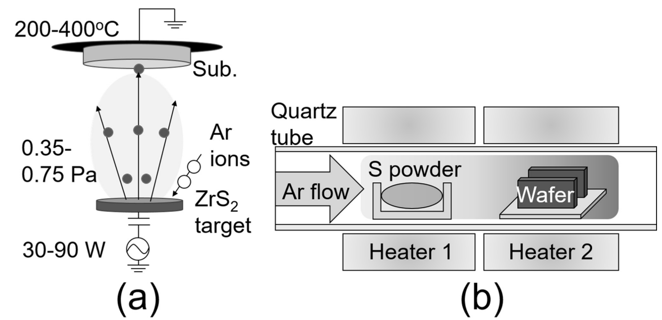


**FIGURE 3.** Schematic diagrams of (a) sputtering tool and (b) sulfur annealing setup. Sputtered samples are sulfurized in sulfur vapor ambient.

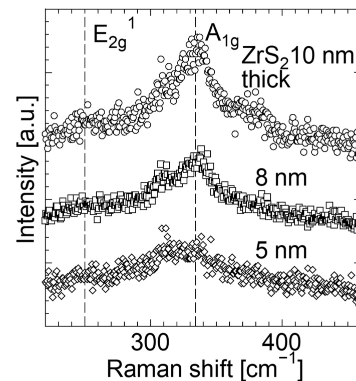


**FIGURE 4.** Raman spectra of $ZrS_2$ films with various thicknesses sputtered with 30 W, 0.55 Pa, 400°C, and annealed at 700°C for 40 min in sulfur vapor ambient. Bulk $E_{2g}^1$ and $A_{1g}$ data [45], [46] are also shown. Intensities have been normalized by silicon peak.

because Raman peak intensities are very sensitive to a film thickness, and a similar phenomenon has been reported in a previous study [46]. The intensity of $ZrS_2$ film decreases with a decrease in a thickness, and the 5 nm $ZrS_2$ peak is hardly observed even after sulfurization at 700°C for 40 min. For further sulfur compensation of $ZrS_2$ film, a dependence on sulfurization temperature was investigated. Fig. 5 shows the Raman spectra of the 10 nm $ZrS_2$ film depending on the annealing temperature. The both $E_{2g}^1$ and $A_{1g}$ peaks increase with an increase in sulfurization temperature. This is because the sulfur compensation and migration of the $ZrS_2$ film were enhanced.

In order to discuss the electrical properties of the $ZrS_2$ film, the Hall-effect mobility and carrier density are evaluated in Figs. 6 to 8. $ZrS_2$ films were prepared some sputtering conditions, and just one temperature at 700°C during sulfur annealing was adopted because the Raman result was effectively improved. In Fig. 6, the Hall-effect mobility decreases and carrier density increases with a decrease in sputter power at less than 70 W. On the other hand, at higher power, they also degraded. This might be because the kinetic energy of $ZrS_2$ particles improves crystallinity and induces damage at lower and higher powers, respectively. In Fig. 7 the Hall-effect mobility decreases and carrier density increases with an increase in pressure to more than 0.55 Pa. On the other hand, they exhibit the same behaviors under pressure

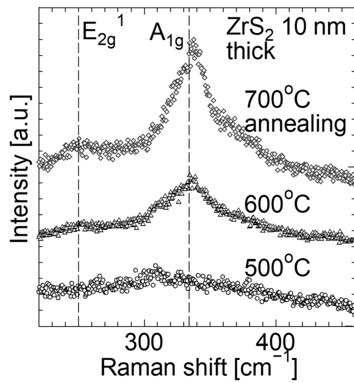


**FIGURE 5. Raman spectra of 10 nm $ZrS_2$ films sputtered with 30 W under 0.55 Pa at 400°C depending on different temperatures of sulfur annealing. Intensities have been normalized by silicon peak.**

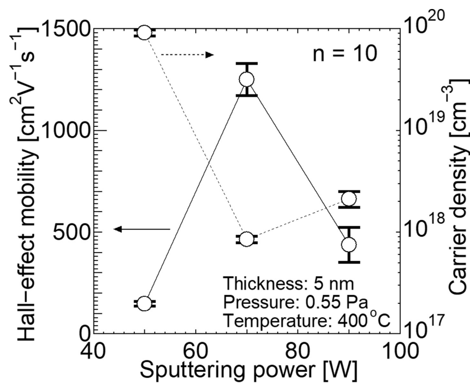


**FIGURE 6. Hall-effect mobility and carrier density of sputtered $ZrS_2$ film depending on sputtering power with mean values and standard errors. Sputtering power was varied under 0.55 Pa at 400°C. Sulfur annealing was applied at 700°C for 40 min. For reference, there is only one report discussing on field effect mobility of ~1 $cm^2V^{-1}s^{-1}$. In order to maximize the performances of $ZrS_2$ film, the dependence on parameters is needed to be precisely controlled.**

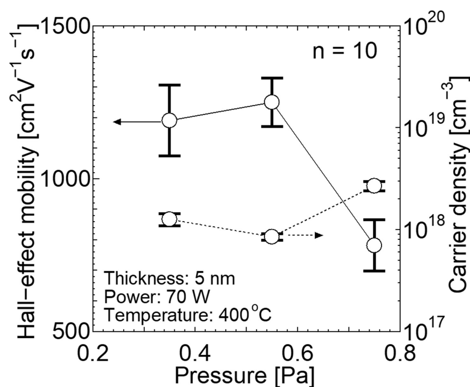


**FIGURE 7. Hall-effect mobility and carrier density of sputtered $ZrS_2$ film depending on argon pressure with mean values and standard errors. Sputtering pressure was varied from base parameters at 400°C with 70 W under 0.55 Pa. Sulfur annealing was applied at 700°C for 40 min.**

slightly less than that. It is speculated that the kinetic energy of sputtered particles is not sufficient to grow under a pressure of more than 0.55 Pa. Below 0.55 Pa, damages in the

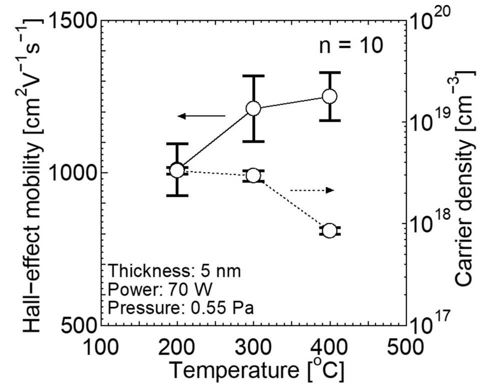


**FIGURE 8. Hall-effect mobility and carrier density of sputtered $ZrS_2$ film depending on substrate temperature with mean values and standard errors. Substrate temperature was varied with 70 W under 0.55 Pa. Sulfur annealing was applied at 700°C for 40 min. The highest mobility of 1,250 $cm^2\ V^{-1}\ s^{-1}$ and the lowest carrier density of 8.5 x $10^{17}$ $cm^{-3}$ in this study are simultaneously achieved.**

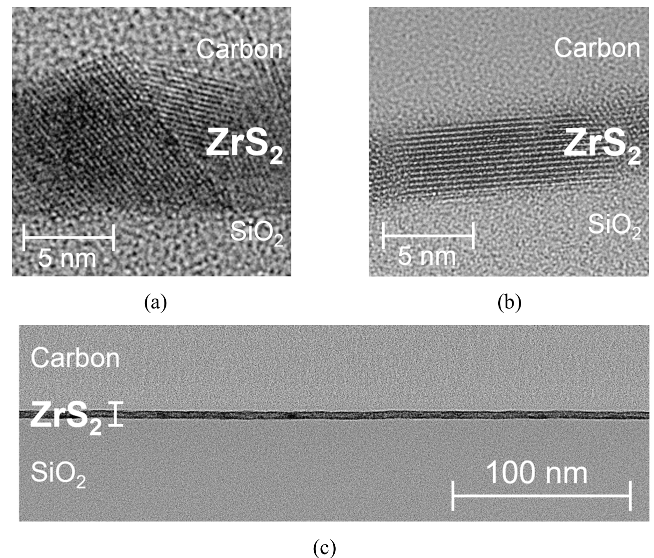


**FIGURE 9. Cross-sectional TEM images of $ZrS_2$ films on $SiO_2$ (a) sputtered at 400°C with sputtering power of 70 W and argon pressure under 0.55 Pa; (b) at room temperature with 60 W and 0.55 Pa. They were annealed in sulfur vapor ambient at 700°C for 40 min; (c) low-magnification image of (b).**

$ZrS_2$ film can be predicted. In Fig. 8 the Hall-effect mobility increases and carrier density decreases with an increase in sputtering temperature. This might be because $ZrS_2$ particles receive the thermal energy from the substrate to migrate. Eventually, the average values of the Hall-effect mobility 1,250 $cm^2\ V^{-1}\ s^{-1}$ and the carrier density 8.5 x $10^{17}$ $cm^{-3}$ were remarkably achieved by using sputtering and sulfur annealing. For repeatability, the similar mobilities and carrier densities are obtained with about 1,200 and 7.0 x $10^{17}$ $cm^{-3}$ in a next lot as average values.

In order to confirm a layered structure of $ZrS_2$ film, cross-sectional transmission electron microscopy (TEM) images were observed in Figs. 9 (a), (b) and (c) under each sputtering conditions. Although a layered $ZrS_2$ film is observed

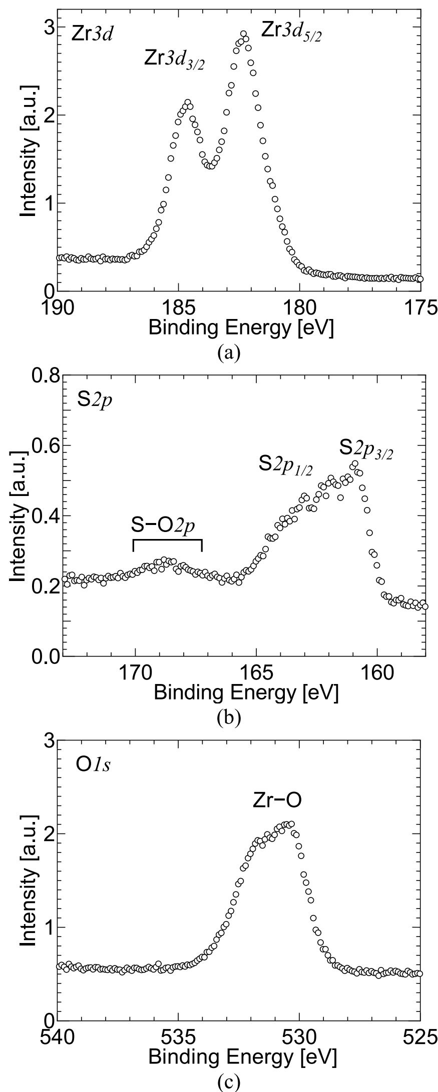


**FIGURE 10. XPS spectra of (a) *Zr3d*, (b) S*2p*, and (c) O*1s* in $ZrS_2$ film sputtered with 60 W under 0.55 Pa at 400°C and annealed in sulfur vapor ambient at 700°C for 40 min.**

even at room temperature in Fig. 9 (a), parallel $ZrS_2$ layers to a $SiO_2$ surface are successfully achieved at a substrate temperature of 400°C in Fig. 9 (b). It is speculated that migration of the $ZrS_2$ film was enhanced by a higher sputtering temperature. However, the grain size is limited up to 15 nm approximately. Fig. 9 (c) is a low-magnified TEM image of (b), and a uniformity of film thickness on the order of micrometers is confirmed.

In order to confirm the thermal stability of $ZrS_2$ film in the air, x-ray photoelectron spectroscopy (XPS) was performed. In Figs. 10 (a) and (b), $Zr3d_{2/3}$, $Zr3d_{5/2}$, $S2p_{3/2}$, and $S2p_{1/2}$ peaks are observed, consistent with reported peaks [47]. On the other hand, peaks of S-O and Zr-O bonds are slightly detected, as shown in Figs. 10 (b) and (c), due to an exposure to the atmosphere [48], [49]. A passivation technique is required to preserve the higher mobility and lower carrier density of atomically-layered $ZrS_2$ film.

## IV. CONCLUSION

The formation of atomic-layered polycrystalline $ZrS_2$ film was successfully performed by sputtering and sulfur annealing. The electrical properties of the $ZrS_2$ film were enhanced by controlling the sputtering parameters, and a Hall-effect mobility of 1,250 $cm^2\ V^{-1}\ s^{-1}$and a carrier density of 8.5 x $10^{17}$ $cm^{-3}$ were remarkably achieved. Advanced MISFETs with $ZrS_2$ film having such good performances are strongly expected for IoT edge devices.

## REFERENCES

[1] W. Zhang, Z. Huang, W. Zhang, and Y. Li, "Two-dimensional semiconductors with possible high room temperature mobility," *Nano Res.*, vol. 7, no. 12, pp. 1731–1737, Jul. 2014. doi: 10.1007/s12274-014-0532-x.

[2] C. Gong, H. Zhang, W. Wang, L. Colombo, R. M. Wallace, and K. Cho, "Band alignment of two-dimensional transition metal dichalcogenides: Application in tunnel field effect transistors," *Appl. Phys. Lett.*, vol. 107, no. 5, Sep. 2015, Art. no. 139904. doi: 10.1063/1.4817409.

[3] Y. Guo and J. Robertson, "Band engineering in transition metal dichalcogenides: Stacked versus lateral heterostructures," *Appl. Phys. Lett.*, vol. 108, no. 23, May 2016, Art. no. 233104. doi: 10.1063/1.4953169.

[4] F. A. Rasmussen and K. S. Thygesen, "Computational 2D materials database: Electronic structure of transition-metal dichalcogenides and oxides," *J. Phys. Chem. C*, vol. 119, no. 23, pp. 13169–13183, Apr. 2015. doi: 10.1021/acs.jpcc.5b02950.

[5] H. Wang *et al.*, "Integrated circuits based on bilayer $MoS_2$ transistors," *Nano Lett.*, vol. 12, no. 9, pp. 4674–4680, Aug. 2012. doi: 10.1021/nl302015v.

[6] B. Radisavljevic, A. Radenovic, J. Brivio, V. Giacometti, and A. Kis, "Single-layer $MoS_2$ transistors," *Nat. Nanotech.*, vol. 6, pp. 147–150, Jan. 2011. doi: 10.1038/NNANO.2010.279.

[7] R. S. Sundaram *et al.*, "Electroluminescence in single layer $MoS_2$," *Nano Lett.*, vol. 13, no. 4, pp. 1416–1421, Mar. 2013. doi: 10.1021/nl400516a.

[8] M. R. Laskar *et al.*, "Large area single crystal (0001) oriented $MoS_2$," *Appl. Phys. Lett.*, vol. 102, no. 25, Jun. 2013, Art. no. 252108. doi: 10.1063/1.4811410.

[9] D. Wickramaratne, F. Zahid, and R. K. Lake, "Electronic and thermoelectric properties of few-layer transition metal dichalcogenides," *J. Chem. Phys.*, vol. 140, no. 12, Mar. 2014, Art. no. 124710. doi: 10.1063/1.4869142.

[10] A. Kuc, N. Zibouche, and T. Heine, "Influence of quantum confinement on the electronic structure of the transition metal sulfide $TS_2$," *Phys. Rev. B, Condens. Matter*, vol. 83, Jun. 2011, Art. no. 245213. doi: 10.1103/PhysRevB.83.245213.

[11] G.-H. Lee *et al.*, "Flexible and transparent $MoS_2$ field-effect transistors on hexagonal boron nitride-graphene heterostuctures," *ACS Nano*, vol. 7, no. 9, pp. 7931–7936, Aug. 2013. doi: 10.1021/nn402954e.

[12] M. Choi, Y. J. Park, B. K. Sharma, S.-R. Bae, S. Y. Kim, and J.-H. Ahn, "Flexible active-matrix organic light-emitting diode display enabled by $MoS_2$ thin-film transistor," *Sci. Adv.*, vol. 4, no. 4, Apr. 2018, Art. no. eaas8721. doi: 10.1126/sciadv.aas8721.

[13] K. He, C. Poole, K. F. Mak, and J. Shan, "Experimental demonstration of continuous electronic structure tuning via strain in atomically thin $MoS_2$," *Nano Lett.*, vol. 13, no. 6, pp. 2931–2936, May 2013. doi: 10.1021/nl4013166.

[14] Y. Wang, C. Cong, C. Qiu, and T. Yu, "Raman spectroscopy study of lattice vibration and crystallographic orientation of monolayer $MoS_2$ under uniaxial strain," *Small*, vol. 9, no. 17, pp. 2857–2861, Sep. 2013. doi: 10.1002/smll.201202876.

[15] A. Azcatl *et al.*, "Covalent nitrogen doping and compressive strain in $MoS_2$ by remote $N_2$ plasma exposure," *Nano Lett.*, vol. 16, no. 9, pp. 5437–5443, Aug. 2016. doi: 10.1021/acs.nanolett.6b01853.

[16] A. Nipane, D. Karmakar, N. Kaushik, S. Karande, and S. Lodha, "Few-layer $MoS_2$ p-type devices enabled by selective doping using low energy phosphorus implantation," *ACS Nano*, vol. 10, no. 2, pp. 2128–2137, Jan. 2016. doi: 10.1021/acsnano.5b06529.

[17] M. R. Laskar *et al.*, "p-type doping of $MoS_2$ thin films using Nb," *Appl. Phys. Lett.*, vol. 104, no. 9, Feb. 2014, Art. no. 092104. doi: 10.1063/1.4867197.
[18] M. Chen *et al.*, "Stable few-layer $MoS_2$ rectifying diodes formed by plasma-assisted doping," *Appl. Phys. Lett.*, vol. 103, no. 4, Oct. 2013, Art. no. 142110. doi: 10.1063/1.4824205.
[19] S. Das, M. Demarteau, and A. Roelofs, "Nb-doped single crystalline $MoS_2$ field effect transistor," *Appl. Phys. Lett.*, vol. 106, no. 17, Apr. 2015, Art. no. 173506. doi: 10.1063/1.4919565.
[20] G. Mirabelli *et al.*, "Back-gated Nb-doped $MoS_2$ junctionless field-effect-transistors," *AIP Adv.*, vol. 6, no. 2, Feb. 2016, Art. no. 025323. doi: 10.1063/1.4943080.
[21] W. Bao, X. Cai, D. Kim, K. Sridhara, and M. S. Fuhrer, "High mobility ambipolar $MoS_2$ field-effect transistors: Substrate and dielectric effects," *Appl. Phys. Lett.*, vol. 102, no. 4, Jan. 2013, Art. no. 042104. doi: 10.1063/1.4789365.
[22] B. Radisavljevic, M. B. Whitwick, and A. Kis, "Small-signal amplifier based on single-layer $MoS_2$," *Appl. Phys. Lett.*, vol. 101, no. 4, Jul. 2012, Art. no. 043103. doi: 10.1063/1.4738986.
[23] H. Qiu, L. Pan, Z. Yao, J. Li, Y. Shi, and X. Wang, "Electrical characterization of back-gated bi-layer $MoS_2$ field-effect transistors and the effect of ambient on their performances," *Appl. Phys. Lett.*, vol. 100, no. 12, Mar. 2012, Art. no. 123104. doi: 10.1063/1.3696045.
[24] D. Jariwala *et al.*, "Band-like transport in high mobility unencapsulated single-layer $MoS_2$ transistors," *Appl. Phys. Lett.*, vol. 102, no. 17, Apr. 2013, Art. no. 173107. doi: 10.1063/1.4803920.
[25] J. Kang, W. Liu, and K. Banerjee, "High-performance $MoS_2$ transistors with low-resistance molybdenum contacts," *Appl. Phys. Lett.*, vol. 104, no. 9, Feb. 2014, Art. no. 093106. doi: 10.1063/1.4866340.
[26] N. Kaushik *et al.*, "Schottky barrier heights for Au and Pd contacts to $MoS_2$," *Appl. Phys. Lett.*, vol. 105, no. 11, Sep. 2014, Art. no. 113505. doi: 10.1063/1.4895767.
[27] D. Sarkar *et al.*, "A subthermionic tunnel field-effect transistor with an atomically thin channel," *Nature*, vol. 526, pp. 91–95, Sep. 2015. doi: 10.1038/nature15387.
[28] X. Zhang *et al.*, "Two-dimensional $MoS_2$-enabled flexible rectenna for Wi-Fi-band wireless energy harvesting," *Nature*, vol. 566, pp. 368–372, Jan. 2019. doi: 10.1038/s41586-019-0892-1.
[29] M. Chhowalla, H. S. Shin, G. Eda, L.-J. Li, K. P. Loh, and H. Zhang, "The chemistry of two-dimensional layered transition metal dichalcogenide nanosheets," *Nat. Chem.*, vol. 5, pp. 263–275, Mar. 2013. doi: 10.1038/NCHEM.1589.
[30] A. Azcatl *et al.*, "$MoS_2$ functionalization for ultra-thin atomic layer deposited dielectrics," *Appl. Phys. Lett.*, vol. 104, no. 11, Mar. 2014, Art. no. 111601. doi: 10.1063/1.4869149.
[31] Y. Li, J. Kang, and J. Li, "Indirect-to-direct band gap transition of the $ZrS_2$ monolayer by strain: First-principles calculations," *RSC Adv.*, vol. 4, no. 15, pp. 7396–7401, 2014. doi: 10.1039/C3RA46090H.
[32] L. Li *et al.*, "Electrical transport and high-performance photoconductivity in individual $ZrS_2$ nanobelts," *Adv. Mater.*, vol. 22, no. 37, pp. 4151–4156, Oct. 2010. doi: 10.1002/adma.201001413.
[33] H. Y. Lv, W. J. Lu, D. F. Shao, H. Y. Lub, and Y. P. Sun, "Strain-induced enhancement in the thermoelectric performance of a $ZrS_2$ monolayer," *J. Mater. Chem. C*, vol. 4, no. 20, pp. 4538–4545, Apr. 2016. doi: 10.1039/C6TC01135G.
[34] G. Fiori *et al.*, "Electronics based on two-dimensional materials," *Nat. Nanotechnol.*, vol. 9, pp. 768–779, Oct. 2014. doi: 10.1038/NNANO.2014.207.
[35] M. Zhang *et al.*, "Controlled synthesis of $ZrS_2$ monolayer and few layers on hexagonal boron nitride," *J. Amer. Chem. Soc.*, vol. 137, no. 22, pp. 7051–7054, May 2015. doi: 10.1021/jacs.5b03807.
[36] X. Wang, L. Huang, X.-W. Jiang, Y. Li, Z. Wei, and J. Li, "Large scale $ZrS_2$ atomically thin layers," *J. Mater. Chem. C*, vol. 4, no. 15, pp. 3143–3148, Mar. 2016. doi: 10.1039/C6TC00254D.
[37] Y. Zhu, X. Wang, M. Zhang, C. Cai, and L. Xie, "Thickness and temperature dependent electrical properties of $ZrS_2$ thin films directly grown on hexagonal boron nitride," *Nano Res.*, vol. 9, no. 10, pp. 2931–2937, Jul. 2016. doi: 10.1007/s12274-016-1178-7.
[38] Y. Shimazu, Y. Fujisawa, K. Arai, T. Iwabuchi, and K. Suzuki, "Synthesis and characterization of zirconium disulfide single crystals and thin-film transistors based on multilayer zirconium disulfide flakes," *ChemNanoMat*, vol. 4, no. 10, pp. 1078–1082, Aug. 2018. doi: 10.1002/cnma.201800304.
[39] T. Ohashi *et al.*, "Multi-layered $MoS_2$ film formed by high-temperature sputtering for enhancement-mode nMOSFETs," *Jpn. J. Appl. Phys.*, vol. 54, no. 4s, Mar. 2015, Art. no. 04DN08. doi: 10.7567/JJAP.54.04DN08.
[40] T. Sakamoto *et al.*, "Mechanism for high hall-effect mobility in sputtered-$MoS_2$ film controlling particle energy," in *Proc. S3S Conf.*, Burlingame, CA, USA, 2018, pp. 1–2. doi: 10.1109/S3S.2018.8640168.
[41] K. Matsuura *et al.*, "Low-carrier-density sputtered $MoS_2$ film by vapor-phase sulfurization," *J. Electron. Mater.*, vol. 47, no. 7, pp. 3497–3501, Jul. 2018. doi: 10.1007/s11664-018-6191-z.
[42] M. Hamada *et al.*, "Hall-effect mobility enhancement of sputtered $MoS_2$ film by vapor phase sulfurization through $Al_2O_3$ passivation film," in *Proc. S3S Conf.*, Burlingame, CA, USA, 2018, pp. 1–2. doi: 10.1109/S3S.2018.8640213.
[43] K. Matsuura *et al.*, "Sputter-deposited-$MoS_2$ *n*MISFETs with top-gate and $Al_2O_3$ passivation under low thermal budget for large area integration," *IEEE J. Electron Devices Soc.*, vol. 6, pp. 1246–1252, Nov. 2018. doi: 10.1109/JEDS.2018.2883133.
[44] K. Matsuura *et al.*, "Normally-off sputtered-$MoS_2$ *n*MISFETs with $MoSi_2$ contact by sulfur powder annealing and ALD $Al_2O_3$ gate dielectric for chip level integration," in *Proc. IWJT*, Kyoto, Japan, 2019, pp. 12–15.
[45] L. Roubi and C. Carlone, "Resonance raman spectrum of $HfS_2$ and $ZrS_2$," *Phys. Rev. B, Condens. Matter*, vol. 37, no. 12, p. 6808, Apr. 1988.
[46] S. Mañas-Valero, V. García-López, A. Cantarero, and M. Galbiati, "Raman spectra of $ZrS_2$ and $ZrSe_2$ from bulk to atomically thin layers," *Appl. Sci.*, vol. 6, no. 9, p. 264, 2016. doi: 10.3390/app6090264.
[47] C. R. Whitehouse, H. P. B. Rimmington, and A. A. Balchin, "Growth conditions and crystal structure parameters of layer compounds in the series $ZrS_xSe_{2-x}$," *Phys. Status Solidi A*, vol. 18, no. 2, pp. 623–631, Aug. 1973. doi: 10.1002/pssa.2210180224.
[48] B. Stypula and J. Stoch, "The characterization of passive films on chromium electrodes by XPS," *Corrosion Sci.*, vol. 36, no. 12, pp. 2159–2167, Dec. 1994. doi: 10.1016/0010-938X(94)90014-0.
[49] C. D. Wagner *et al.*, "Auger and photoelectron line energy relationships in aluminum–oxygen and silicon–oxygen compounds," *J. Vac. Sci. Technol.*, vol. 21, no. 4, p. 933, 1982. doi: 10.1116/1.571870.

**MASAYA HAMADA** received the M.E. degree in electrical engineering from the Tokyo Institute of Technology, Japan, in 2019, where he is currently pursuing the Doctoral degree.

**KENTARO MATSUURA** received the B.E. and M.E. degrees in electrical engineering from the Tokyo Institute of Technology, Japan, in 2015 and 2017, respectively, where he is currently pursuing the Doctoral degree.

**TAKURO SAKAMOTO** received the M.E. degree in electrical engineering from the Tokyo Institute of Technology, Japan, in 2019.

**IRIYA MUNETA** (M'16) received the B.E., M.E., and Ph.D. degrees in engineering from the University of Tokyo in 2009, 2011, and 2014, respectively, where he was a Post-Doctoral Researcher for two years. During those periods, he thoroughly investigated molecular beam epitaxy, materials science, and electronic devices of ferromagnetic semiconductors. He joined the Tokyo Institute of Technology in 2016, where he is currently an Assistant Professor. His current research is focused on 2-D materials and transition metal dichalcogenides, especially on deposition of thin films, materials science, and device integration of them.

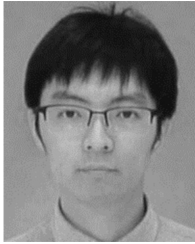

**TAKUYA HOSHII** (M'10) received the B.S., M.S., and Ph.D. degrees in engineering from the University of Tokyo, Tokyo, Japan, in 2006, 2008, and 2011, respectively.

He is currently an Assistant Professor with the Tokyo Institute of Technology, Yokohama, Japan.

**KUNIYUKI KAKUSHIMA** (M'99) received the B.S., M.S., and Ph.D. degrees in electrical engineering from the University of Tokyo, Tokyo, Japan, in 1999, 2001, and 2004, respectively.

He is currently an Associate Professor with the Tokyo Institute of Technology, Yokohama, Japan.

**KAZUO TSUTSUI** (M'02–SM'07) received the B.E., M.E., and Ph.D. degrees in electrical engineering from the Tokyo Institute of Technology, Yokohama, Japan, in 1981, 1983, and 1986, respectively.

He is currently with the Tokyo Institute of Technology.

**HITOSHI WAKABAYASHI** (M'00) received the M.E. and Ph.D. degrees in electrical engineering from the Tokyo Institute of Technology, Japan, in 1993 and 2003, respectively. He was with NEC Corporation from 1993 to 2006, the Massachusetts Institute of Technology from 2000 to 2001, and Sony Corporation from 2006 to 2012. He has been with the Tokyo Institute of Technology since 2013. He was a recipient of the Young Scientist Presentation Award 2000 of JSAP. He has served as the General Chair for Symposium on VLSI Technology 2013, EDTM 2018, and IWJT 2017/2019.